

Lasing properties of non-polar GaN quantum dots in cubic aluminum nitride microdisk cavities

M. Bürger,^{1,a)} G. Callsen,² T. Kure,² A. Hoffmann,² A. Pawlis,¹ D. Reuter,¹ and D. J. As¹

¹Universität Paderborn, Department Physik, Warburger Str. 100, 33098 Paderborn, Germany

²Institut für Festkörperphysik, Technische Universität Berlin, Hardenbergstr. 36, 10623 Berlin, Germany

(Received 24 May 2013; accepted 23 June 2013; published online 9 July 2013)

We demonstrate laser emission from optically pumped non-polar cubic GaN quantum dots embedded in cubic aluminum nitride microdisks. Power dependent micro-photoluminescence studies at low temperature (~ 10 K) revealed S-shaped curves of the integral mode intensity. We observed whispering gallery modes with quality factors up to 5000 at the high energy side (4 eV, i.e., ~ 310 nm wavelength) in photoluminescence spectra of microdisks with a diameter of $2.5 \mu\text{m}$. Furthermore, we have determined the spontaneous emission coupling factors to $\beta = 0.12$ and $\beta = 0.42$ for resonator modes of different radial orders. © 2013 AIP Publishing LLC.

[<http://dx.doi.org/10.1063/1.4813408>]

Recently, optical microcavities (e.g., microdisks, nanorods, photonic crystal cavities) based on group III-nitrides have attracted large interest as they offer promising properties for applications in quantum information technology extending from single photon sources to low threshold cavity lasers.^{1–3} Since the discovery of whispering gallery modes (WGMs) by Lord Rayleigh in the last century, considerable efforts were made towards the generation of WGMs in semiconductor microdisks.^{4,5} Microdisks containing quantum dots (QDs) as active material combine the benefits of a small mode volume as well as a zero dimensional electron density of states. Such features lead to low threshold-power and highly gained lasers. QD microdisk lasers have been realized from the infrared employing InGaAs QDs up to blue light emission based on CdSe QDs.^{6,7} Group III-nitride microresonators are promising for light sources that extend the spectral range towards the ultraviolet. High quality wurtzite GaN/AlN microcavities containing QDs have been fabricated, and quality factors (Q-factors, $Q = \frac{E}{\Delta E}$) exceeding 7000 in microdisks⁸ and 5000 in photonic crystal cavities,⁹ respectively, have been reported up to now. These high Q-factors of the GaN/AlN microcavities result from optimized etching technology and high crystal quality.

However, in naturally stable wurtzite GaN the Quantum Confined Stark Effect arises due to internal piezoelectric and spontaneous polarization fields along the polar (0001) c-direction. These built-in electric fields lead to a spatial separation of the electrons and holes. As a consequence, the electron-hole recombination probability is reduced, which limits the performance of optoelectronic devices containing hexagonal GaN QDs or quantum wells (QWs). Hence, radiative lifetimes ranging from several 100 ps up to several μs are observed.¹⁰ A promising approach to avoid internal fields is the growth of metastable cubic group III-nitrides along the (001) direction on cubic silicon carbide substrates.¹¹ The radiative recombination time of cubic GaN (c-GaN) QDs compared to wurtzite GaN QDs can be two orders of

magnitude lower.^{12,13} Another feature of c-GaN QDs is the long exciton spin lifetime that allows spin conversations even at room temperature.¹⁴ Therefore, c-GaN QDs provide a large coupling of the emission to the photonic WGMs of the microdisk, a key requirement for efficient optical resonators. The enhancement of the QD emission is described by the Purcell Effect.¹⁵ Cubic GaN QD emitters are promising for laser applications in the ultraviolet spectral range. Up to now, lasing has been achieved in hexagonal microdisks containing bulk GaN and InGaN quantum wells.^{16,17}

In this work, we investigate the emission properties of cubic AlN (c-AlN) microdisks containing a single layer of non-polar c-GaN QD emitters. Our samples were grown by plasma assisted molecular beam epitaxy (PAMBE). Electron beam lithography followed by two consecutive reactive ion etching (RIE) steps was used to fabricate freestanding c-AlN slabs on a 3C-SiC substrate post.¹⁸ The optical characterization of the microdisks in the high energy range of 3.2 to 4.2 eV was performed by micro-photoluminescence (μ -PL) measurements at low temperature (~ 10 K). The lasing properties of WGMs in the high energy tail of the spectrum were studied in detail by power dependent μ -PL measurements.

For the PAMBE growth of our samples, $10 \mu\text{m}$ 3C-SiC pseudo substrates on top of $500 \mu\text{m}$ Si (001) were used.¹⁹ The active material consists of a single c-GaN QD layer enclosed in two 30 nm thick c-AlN barriers. In order to form self assembled QDs by the Stranski Krastanov (SK) growth mode, approximately 4 monolayers of GaN were deposited on the c-AlN buffer layer.²⁰ The c-AlN/c-GaN growth was performed at a growth temperature of 760°C . The QD densities of uncapped samples were investigated by scanning atomic force microscopy (AFM) measurements and result densities are in the order of 10^{11}cm^{-2} .²¹ Details about the growth of c-GaN/c-AlN are given in former work.^{20,22,23}

Prior to the microdisk patterning, the sample surface was covered by an 80 nm thick SiO_2 etching mask. Afterwards, electron beam lithography was performed in order to define structures of different circular shapes. The freestanding 60 nm thin microdisks were patterned by a two step RIE process using SiCl_4 and Ar plasma for the active layer in step one. The second step consisted of CF_4 chemistry

^{a)}Author to whom correspondence should be addressed. Electronic mail: mbuerger@mail.uni-paderborn.de. Tel. +495251605831. Fax: +495251605843.

for selective 3C-SiC substrate etching to realize an undercut of the c-AlN slab. To achieve isotropic 3C-SiC etching, the substrate was heated up to 375 °C.

The microdisks were optically characterized in a μ -PL setup. As excitation source the fourth harmonic of a Nd:YAG laser (Coherent Antares 76s) at 266 nm (i.e., 4.66 eV) with a pulse length of 60 ps was applied. The laser beam was focused by a microscope objective (numerical aperture 0.4) resulting in a laser spot with a diameter of $\sim 1 \mu\text{m}$. The emission was collected by the same objective and a 1 m monochromator (Spex 1704) with a spectral resolution of $\sim 300 \mu\text{eV}$ was used as a dispersing element. A piezo adjustable objective enables μ -PL measurements of single microdisks.

As the excitation energy (4.66 eV) is below the c-AlN bandgap (direct bandgap 5.93 eV, indirect bandgap 5.3 eV),^{24,25} carrier excitation in the barriers is negligible, resulting in a weak absorption in our samples limited to the region of the single QD layer. Using dielectric constants of $\epsilon_1 = 7$ and $\epsilon_2 = 1.8$, we calculated the absorption coefficient to $\alpha_{\text{c-GaN}} = 0.012 \text{ nm}^{-1}$ at 4 eV.²⁶ Taking a height z for the QDs into account, the absorption can be derived by $I(z) = I_0 \exp(-\alpha_{\text{c-GaN}}z)$. Assuming a height of $z \cong 3 \text{ nm}$ for the QDs,²¹ the absorbed power in the active layer can be estimated to $\sim 4\%$ and additional loss due to reflection at the sample surface may be $\sim 13\%$.^{24,27} The excitation powers given in the following diagrams were corrected according to this approximation.

Fig. 1(a) displays a PL spectrum of a $2.5 \mu\text{m}$ microdisk. A Gaussian shaped emission band with a FWHM of 228 meV peaking at 3.63 eV is observed and is attributed to the QD ensemble luminescence.^{28,29} Most of the QD emission is not in resonance with one of the WGMs of the microdisk, which leads to the broad QD ensemble emission

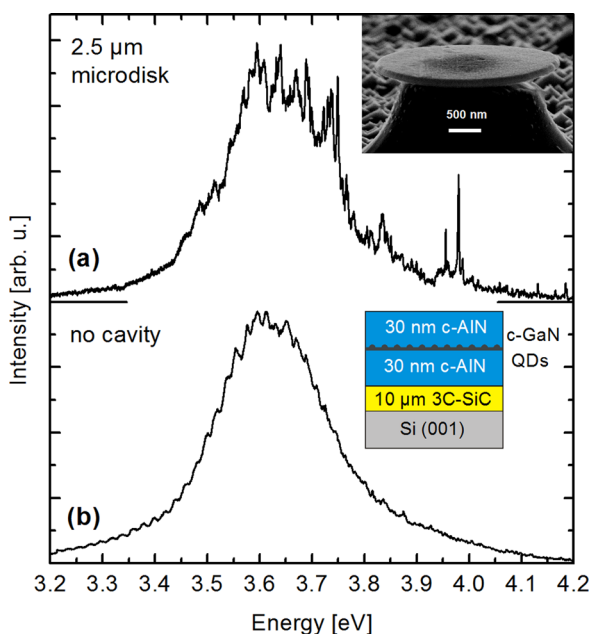


FIG. 1. PL spectra taken at $\sim 10 \text{ K}$ of a $2.5 \mu\text{m}$ microdisk (a) and for reference, of an unprocessed part of the sample (b) in the range from 3.2 eV to 4.2 eV. Insets: (top) Side view scanning electron microscopy image of a typical $2.5 \mu\text{m}$ microdisk and a schematic structure of our epitaxial layers (bottom).

band. Owing to the high quantum density in our samples, the broad emission band is correlated to the size distribution of the QDs.³⁰ The overall spectrum is superimposed by several sharp peaks, which are assigned to an enhancement of the emission of QDs resonant with WGMs.

The most dominant modes occur on the high energy side of the emission band. For energies $E \leq 3.55 \text{ eV}$, scattering of the circulating wave at imperfections of the sidewalls is more dominant and inhibits the appearance of WGMs on the low energy side.^{6,31} The inset of Fig. 1(a) shows a freestanding microdisk of $2.5 \mu\text{m}$ diameter on top of a 3C-SiC post. We attribute imperfections in form of vertical striations at the sidewall as well as etch pits at the surface to mask erosion during the etching of the active layer. The PL spectrum of an unprocessed part of the sample is dominated by an emission band of the QD ensemble at 3.63 eV (Fig. 1(b)). Apart from Fabry-Pérot layer oscillations of the $10 \mu\text{m}$ 3C-SiC substrate, which superimpose the reference spectrum, no WGMs are identified. A schematic sketch of the layer sequence of our unpatterned samples is given in the inset of Fig. 1(b).

In the following, we focus on the evaluation of the lasing emission of particular WGMs. Fig. 2 illustrates the excitation power dependence of the emission of a $2.5 \mu\text{m}$ microdisk in the high energy range between 3.88 eV and 4.00 eV for 5 different excitation powers increasing from 5 kW cm^{-2} to 720 kW cm^{-2} . The analyzed modes at $E = 3.90 \text{ eV}$ (mode 1 in Fig. 2) and $E = 3.98 \text{ eV}$ (mode 2 in Fig. 2), respectively, are highlighted in grey. For a low excitation power of 5 kW cm^{-2} , the resonator modes appear with weak intensities and denote a linear increase with higher power up to $30\text{--}40 \text{ kW cm}^{-2}$. As the excitation power was further increased, clearly sharp WGMs dominate the spectra, cf. Fig. 2.

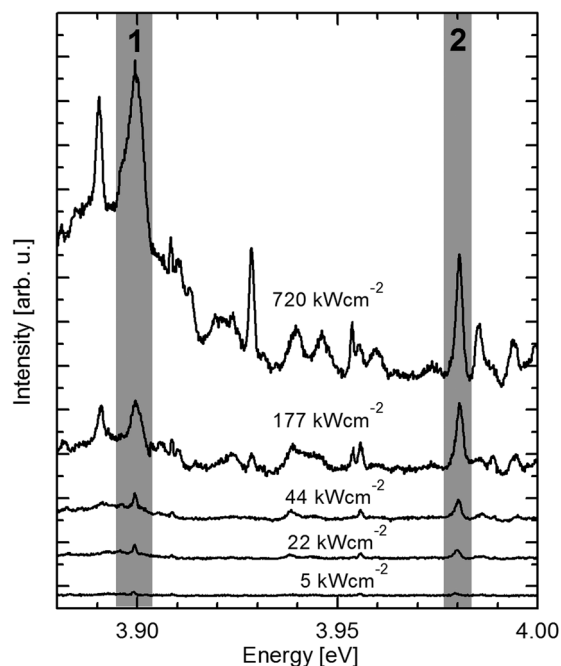


FIG. 2. Power dependent PL spectra of the high energy region of the QD ensemble spectrum. The excitation density was increased from 5 kW cm^{-2} to 720 kW cm^{-2} . The analyzed lasing modes at $E = 3.90 \text{ eV}$ (mode 1) and $E = 3.98 \text{ eV}$ (mode 2) are highlighted in grey.

The total integrated intensity of the QD ensemble (see Fig. 1(a)) is directly related to the QD density ($\sim 10^{11} \text{ cm}^{-2}$ in a single layer of c-GaN QDs), which we obtained from the AFM measurements.²¹ By considering a laser spot with $1 \mu\text{m}$ diameter less than 1000 QDs contribute to the luminescence of the ensemble. Consequently, the ratio of the integrated intensity of the lasing modes versus that of the QD ensemble allows us to approximate the average number of QDs that couple to one lasing mode. In this way, the number of QDs estimated is about 1–10 QDs per mode. Therefore, we quantify the relatively low intensities of the resonantly enhanced emission compared to that of the QD ensemble to the small number of QDs which couple into a lasing mode. Notably in this context, it might render possible to implement a micro-disk laser based on a single QD emitting in the lasing mode. However, in practice, more QDs contribute to the lasing mode of our microdisk samples, due to significant nonresonant coupling of adjacent QDs.³²

Fig. 3 depicts the integrated mode intensity obtained from modes 1 and 2 as a function of the excitation power in a double logarithmic scale. The experimental data are indicated by dots and the asymptotes for low and high power are drawn in dashed lines. Each mode area was determined without the underlying fraction of the spontaneous emission by a Lorentz fit of the respective lasing mode.²⁷ For both modes, a clearly S-shaped threshold behavior is observed. Such emission characteristics are typical for semiconductor microcavity lasers with a small mode volume.^{7,33,34} The transition from nonlasing to lasing starts at $\sim 30 \text{ kW cm}^{-2}$ for mode 1 and at $\sim 20 \text{ kW cm}^{-2}$ for mode 2, respectively. The fraction

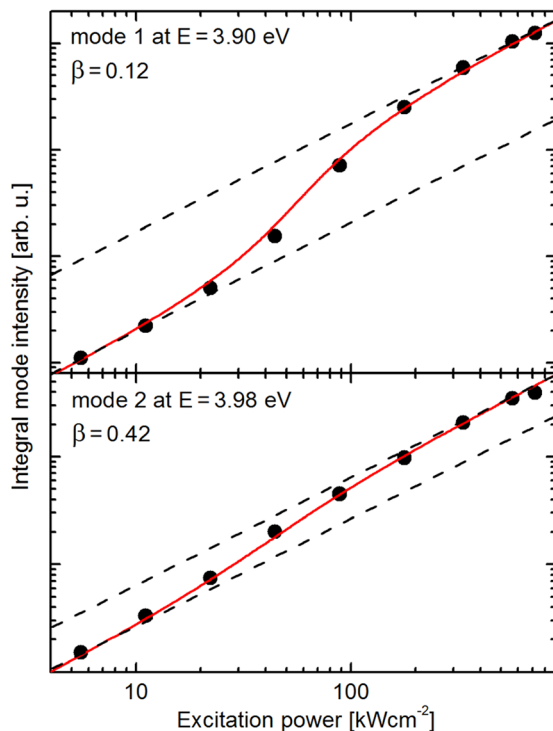


FIG. 3. Plot of the integral mode intensity versus the excitation power of the lasing modes at $E = 3.90 \text{ eV}$ and $E = 3.98 \text{ eV}$ in a double logarithmic scale. The experimental results are indicated by dots, the solid lines display fits according to the theoretical model.³³ The dashed lines show the low and high power asymptotes.

of the spontaneous emission that couples into the lasing mode is described by the β -factor. The small offset between low and high power operation suggests high β values compared to that of conventional lasers and results from the small number of QDs coupling into the WGM. Mode 1 exhibits a smaller β -factor of 0.12 compared to mode 2 with a β -factor of 0.42.

Björk and Yamamoto derived a theoretical model to analyze semiconductor microcavity lasers.³³ Based on this model, the emission intensity as a function of the excitation power can be described analytically by

$$I = \frac{q\gamma}{\beta} \left[\frac{p}{1+p} (1 + \xi)(1 + \beta p) - \xi \beta p \right], \quad (1)$$

for negligible nonradiative losses, where I is the pumping rate, q the electron charge, and p denotes the mean photon number in the cavity. The properties of the cavity and the active material are represented by the photon escape rate γ from the cavity. The mean number of emitted photons in the cavity is described by ξ . In our case, the analytical model confirms the experimental results using $\gamma = 5$ and 15 and $\xi = 0.35$ and 0.1 for modes 1 and 2, respectively. The fitted curves are indicated by solid lines in Fig. 3.

Furthermore, we calculated theoretical mode spectra from three dimensional finite difference time domain simulations with corresponding mode profiles to determine the radial order of modes 1 and 2.^{18,35} Thereby, we assign mode 1 to a second and mode 2 to a first radial order WGM. The second order mode 1 has a larger mode volume and covers more space in the disk periphery, which usually results in a weaker coupling between the QDs and the resonator modes. This becomes obvious when we compare the smaller β -factor of 0.12 for mode 1 with the higher β -factor of 0.42 for mode 2.

In general, the measured Q value of the WGMs can be described by²⁷

$$Q_{\text{tot}}^{-1} = Q_{\text{rad}}^{-1} + Q_{\text{abs}}^{-1} + Q_{\text{loss}}^{-1}, \quad (2)$$

where Q_{rad}^{-1} is related to radiation loss from a perfect disk, Q_{abs}^{-1} is determined by optical absorption of the active medium, and Q_{loss}^{-1} characterizes scattering losses due to imperfections of the disk surfaces and sidewalls. Close to the threshold power, when optical transparency is reached, the absorption of the QDs becomes negligible. In our case, scattering losses at the disk sidewall and surfaces can be assumed as the dominant loss mechanism.³¹

Fig. 4 shows the linewidth versus the excitation power of lasing mode 2 at $E = 3.98 \text{ eV}$. The accuracy was estimated to be $\pm 0.3 \text{ meV}$. At low excitation powers, the mode exhibits a narrowing linewidth until the lasing threshold is crossed. This narrowing is explainable in terms of the Schawlow Townes model, which describes an inverse dependence of the linewidth compared to the optical power output of the lasing mode ($\Delta E \sim \frac{1}{P_0}$).³⁶ Around transparency, we measure a linewidth of 0.8 meV resulting in a cavity Q of ~ 5000 . Above threshold, the linewidth increases to 4.6 meV . We attribute this FWHM increase to free carrier absorption.^{37,38} Since most of the QDs are not lasing, large carrier densities at high

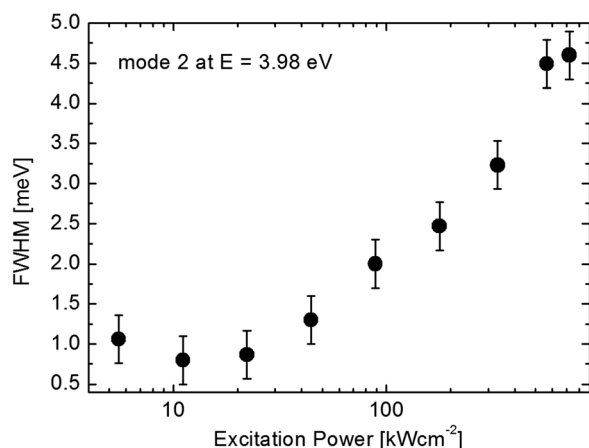


FIG. 4. FWHM of mode 2 at $E = 3.98$ eV as a function of the excitation power.

excitation powers also lead to changes of the refractive index and influence thereby the linewidth of the WGMs.^{39,40}

In summary, we have fabricated cubic AlN microdisks containing a single layer of self assembled non-polar cubic GaN QDs. The microdisks were patterned by electron beam lithography and two consecutive dry chemical etching steps. Lasing properties of a $2.5 \mu\text{m}$ diameter microdisk were analyzed at different excitation powers in μ -PL studies at low temperatures. Typical S-shaped output characteristics for semiconductor microcavity lasers were obtained. The onset of lasing was observed at a threshold of 20 kW cm^{-2} and we obtained cavity modes with Q-factors up to ~ 5000 . Furthermore, we determined the fraction of spontaneous emission coupling into a WGM of radial orders 1 and 2 to $\beta = 0.12$ and $\beta = 0.42$, respectively. The results presented here demonstrate the strong potential of cubic AlN/GaN QDs in microdisk resonator structures for low-threshold power lasers in the ultraviolet spectral range.

This work was supported by the DFG graduate program GRK 1464 “Micro- and Nanostructures in Optoelectronics and Photonics” and the Collaborative Research Center (SFB 787).

¹A. C. Tamboli, E. D. Haberer, R. Sharma, K. H. Lee, S. Nakamura, and E. L. Hu, *Nat. Photonics* **1**, 61 (2007).

²K. J. Vahala, *Nature* **424**, 839 (2003).

³S. P. Chang, K. P. Sou, C. H. Chen, Y. J. Cheng, J. K. Huang, C. H. Lin, H. C. Kuo, C. Y. Chang, and W. F. Hsieh, *Opt. Express* **20**, 12457 (2012).

⁴Lord Rayleigh, *Philos. Mag.* **20**, 1001 (1910).

⁵S. L. McCall, A. F. J. Levi, R. E. Slusher, S. J. Pearton, and R. A. Logan, *Appl. Phys. Lett.* **60**, 289 (1992).

⁶E. Peter, I. Sagnes, G. Guirleo, S. Varoutsis, J. Bloch, A. Lemaître, and P. Senellart, *Appl. Phys. Lett.* **86**, 021103 (2005).

⁷J. Renner, L. Worschech, A. Forchel, S. Mahapatra, and K. Brunner, *Appl. Phys. Lett.* **89**, 231104 (2006).

⁸M. Mexis, S. Sergent, T. Guillet, C. Brimont, T. Bretagnon, B. Gil, F. Semond, M. Leroux, D. Néel, S. David, X. Chécoury, and P. Boucaud, *Opt. Lett.* **36**, 2203 (2011).

⁹S. Sergent, M. Arita, S. Kako, S. Iwamoto, and Y. Arakawa, *Appl. Phys. Lett.* **100**, 121103 (2012).

¹⁰S. Kako, M. Miyamura, K. Tachibana, K. Hoshino, and Y. Arakawa, *Appl. Phys. Lett.* **83**, 984 (2003).

¹¹D. J. As, *Microelectron. J.* **40**, 204 (2009).

¹²J. Simon, N. T. Pelekanos, C. Adelman, E. Martinez-Guerrero, R. André, B. Daudin, L. S. Dang, and H. Mariette, *Phys. Rev. B* **68**, 035312 (2003).

¹³T. Bretagnon, P. Lefebvre, P. Valvin, R. Bardoux, T. Guillet, T. Taliercio, and B. Gil, *Phys. Rev. B* **73**, 113304 (2006).

¹⁴D. Lagarde, A. Balocchi, H. Carrère, P. Renucci, T. A. X. Marie, S. Founta, and H. Mariette, *Phys. Rev. B* **77**, 041304(R) (2008).

¹⁵A. Kiraz, P. Michler, C. Becher, B. Gayral, A. Imamoglu, L. Zhang, E. Hu, W. V. Schoenfeld, and P. M. Petroff, *Appl. Phys. Lett.* **78**, 3932 (2001).

¹⁶H. W. Choi, K. N. Hui, P. T. Lai, P. Chen, X. H. Zhang, S. Tripathy, J. H. Teng, and S. J. Chua, *Appl. Phys. Lett.* **89**, 211101 (2006).

¹⁷E. D. Haberer, R. Sharma, C. Meier, A. R. Stonas, S. Nakamura, S. P. DenBaars, and E. L. Hu, *Appl. Phys. Lett.* **85**, 5179 (2004).

¹⁸M. Bürger, M. Ruth, S. Declair, J. Förstner, C. Meier, and D. J. As, *Appl. Phys. Lett.* **102**, 081105 (2013).

¹⁹T. Chassagne, A. Leycuras, C. Balloud, P. Arcade, H. Peyre, and S. Juillaguet, *Mater. Sci. Forum* **457–460**, 273 (2004).

²⁰T. Schupp, T. Meisch, B. Neuschl, M. Feneberg, K. Thonke, K. Lischka, and D. J. As, *AIP Conf. Proc.* **1292**, 165 (2010).

²¹M. Bürger, T. Schupp, K. Lischka, and D. J. As, *Phys. Status Solidi C* **9**(5), 1273 (2012).

²²T. Schupp, K. Lischka, and D. J. As, *J. Cryst. Growth* **312**, 1500 (2010).

²³E. Martinez-Guerrero, C. Adelman, F. Chabuel, J. Simon, N. T. Pelekanos, G. Mula, B. Daudin, G. Feuillet, and H. Mariette, *Appl. Phys. Lett.* **77**, 809 (2000).

²⁴M. Röppischer, R. Goldhahn, G. Rossbach, P. Schley, C. Cobet, N. Esser, T. Schupp, K. Lischka, and D. J. As, *J. Appl. Phys.* **106**, 076104 (2009).

²⁵P. Jonnard, N. Capron, F. Semond, J. Massies, E. Martinez-Guerrero, and H. Mariette, *Eur. Phys. J. B* **42**, 351 (2004).

²⁶M. Feneberg, M. Röppischer, C. Cobet, N. Esser, J. Schörmann, T. Schupp, D. J. As, F. Hörich, J. Bläsing, A. Krost, and R. Goldhahn, *Phys. Rev. B* **85**, 155207 (2012).

²⁷R. E. Slusher, A. F. J. Levi, U. Mohideen, S. L. McCall, S. J. Pearton, and R. A. Logan, *Appl. Phys. Lett.* **63**, 1310 (1993).

²⁸T. Schupp, K. Lischka, and D. J. As, *J. Cryst. Growth* **323**, 286 (2011).

²⁹D. J. As, F. Schmilgus, C. Wang, B. Schöttker, D. Schikora, and K. Lischka, *Appl. Phys. Lett.* **70**, 1311 (1997).

³⁰G. Schmid, *Nanoparticles: From Theory to Application* (Wiley-VCH, New York, 2006).

³¹S. Sergent, J. C. Moreno, E. Frayssinet, Y. Laaroussi, S. Chenot, J. Renard, D. Sam-Giao, B. Gayral, D. Néel, and S. David, *J. Phys.: Conf. Ser.* **210**, 012005 (2010).

³²K. Hennessy, A. Badolato, M. Winger, D. Gerace, M. Atatüre, S. Gulde, S. Fält, E. L. Hu, and A. Imamoglu, *Nature* **445**, 896 (2007).

³³G. Björk and Y. Yamamoto, *IEEE J. Quantum Electron.* **27**, 2386 (1991).

³⁴M. Witzany, R. Roßbach, W.-M. Schulz, M. Jetter, P. Michler, T.-L. Liu, E. Hu, J. Wiersig, and F. Jahnke, *Phys. Rev. B* **83**, 205305 (2011).

³⁵S. Declair, C. Meier, T. Meier, and J. Förstner, *Photonics Nanostruct. Fundam. Appl.* **8**, 273 (2010).

³⁶A. L. Schawlow and C. H. Townes, *Phys. Rev.* **112**, 1940 (1958).

³⁷B. Gayral, J. M. Gérard, A. Lemaître, C. Dupuis, L. Manin, and J. L. Pelouard, *Appl. Phys. Lett.* **75**, 1908 (1999).

³⁸D. K. Young, L. Zhang, D. D. Awschalom, and E. L. Hu, *Phys. Rev. B* **66**, 081307 (2002).

³⁹D. Welford and A. Mooradian, *Appl. Phys. Lett.* **40**, 560 (1982).

⁴⁰K. Vahala and A. Yariv, *Appl. Phys. Lett.* **43**, 140 (1983).